Journal of Materials Chemistry A

Accepted Manuscript

ROYAL SOCIETY OF CHEMISTRY

www.rsc.org/materialsA

Table of contents entry

Recharging of a fully discharged Li/FeS battery does not reconstitute the original FeS structure, further cycling is co-contributed by the Li_2S/Li_2S_n and Fe/FeS redox couples and affected by the electrolyte solvent and charging cutoff voltage.

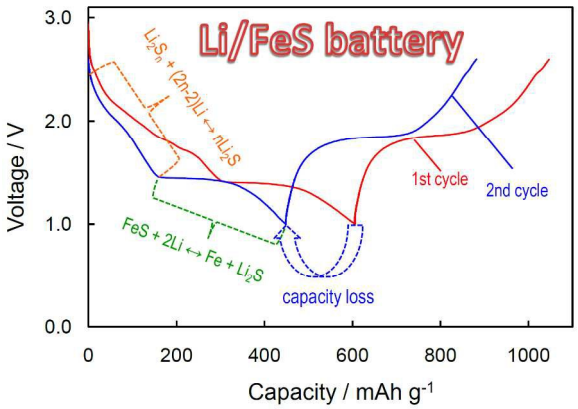

Cite this: DOI: 10.1039/c0xx00000x

www.rsc.org/xxxxxx

PAPER

Chemical stability and electrochemical characteristics of FeS microcrystals as the cathode material of rechargeable lithium battery

Dat T. Tran[a] and Sheng S. Zhang[a]*

Received (in XXX, XXX) Xth XXXXXXXXX 20XX, Accepted Xth XXXXXXXXX 20XX

DOI: 10.1039/b000000x

Carbon precursor coated iron monosulphide (CP@FeS) microcrystals are synthesized by a facile one-pot solvothermal reaction of $FeSO_4$ and twice moles of Na_2S with sucrose as the carbon source, and evaluated as the cathode material of rechargeable lithium batteries. Results show that the obtained CP@FeS microcrystals consist of two FeS phases and contain small amount of sulphur. In storage, FeS transforms into Fe_3S_4, which is further oxidized by oxygen in air to release elemental sulphur. Interestingly, such transformation and oxidization are found only to affect the first discharge voltage profile with negligible impact on the specific capacity and cycling performance of Li/FeS battery. It is shown that the cyclability of Li/FeS battery is greatly affected by the electrolyte solvent and charging cutoff voltage. In this paper, we discuss the chemical stability and redox mechanism of the FeS cathode material, and investigate the factors that affect the cycling performance of Li/FeS batteries.

1. Introduction

Cost, performance and safety are three essential elements to determine the success of rechargeable batteries in applications of the transportation and stationary smart grid. In the near future, compromising of these three elements has been considered to be the most viable approach.[1] For this reason, much research attention has recently been focused on the battery systems beyond Li ion, which are featured by the high specific capacity and moderate operation voltage. These batteries typically use a conversion-type cathode material whose redox involves the transfer of multiple electrons, such as oxygen for Li-air battery and sulphur for Li-S battery. Other conversion-type cathode materials include transition metal oxides, sulphides, halides, and nitrides, among which iron monosulphide is of particular interest because of its cost effectiveness, low environmental impact and natural abundance.[2-6] By the nature, iron monosulphide is a nonstoichiometric compound having a general formula of Fe_mS with m=0.91~1.15 or FeS_n with n=0.87~1.10, and for simplicity it is often referred to as FeS in textbook[7]. Energy storage of FeS in lithium batteries is based on a reversible displacement reaction of "$2Li + FeS \leftrightarrow Fe + Li_2S$", which corresponds to a theoretical capacity of 610 mAh g^{-1} at an averaged potential of 1.5 V vs. Li/Li^+. In early stage of the study, the FeS was proposed as the cathode material of rechargeable lithium batteries,[3, 8, 9] and recently the scope has extended to the anode material of Li-ion batteries.[10-15] Although operating at relatively low potentials, FeS is still considered to be very promising for the cathode material in consideration of its high specific capacity, excellent safety, natural abundance, and low environmental impact.

Key challenge for the Li/FeS batteries is the poor cyclability, which is to great extent associated with the large volume change (up to 200%) and the formation of soluble polysulphide taking place during the conversion reaction.[3, 15] For these problems, the reduction of FeS particle size has been taken to alleviate the mechanical stress caused by the volume change, and the coating with conductive carbon has been used to protect the dissolved polysulphide from diffusion out of the cathode.[11, 12, 14] Fundamentally, some unique phenomena that are frequently observed from the Li/FeS batteries are poorly understood. For example, there is a significant loss in the capacity from the 1st discharge to 2nd discharge, and the voltage profile of the first discharge cannot be reproduced by recharging whereas the results reported by different research groups vary vastly.[3, 12, 13, 15] In order to improve the performance of Li/FeS batteries and understand their unique phenomena, in this work we attempt to synthesise a carbon-coated FeS cathode material by using a facile one-pot solvothermal reaction with sucrose as the carbon source. Result turns out that the solvothermal pyrolysis of sucrose does not produce conductive carbon, instead forms a carbon precursor. Therefore, we refer to our product as the carbon precursor coated iron monosufide (CP@FeS). We here evaluate the factors that greatly affect the cyclability of Li/FeS batteries and discuss the chemical stability and redox mechanism of the FeS cathode material.

2. Experimental

2.1. Synthesis and characterization of CP@FeS

Starting materials, $FeSO_4{\cdot}7H_2O$ (Alfa Aesar), $Na_2S{\cdot}9H_2O$ (Sigma-Aldrich), sucrose (Alfa Aesar) and ethanol (Sigma-Aldrich), were used as received. To make CP@FeS, 2.0 g (7.19 mmol) $FeSO_4{\cdot}7H_2O$ and 0.216 g sucrose were dissolved into 7.5 mL deionized water in a beaker, and 3.45 g (14.40 mmol) $Na_2S{\cdot}9H_2O$

was dissolved into 7.5 mL deionized water in the other beaker, then two solutions were mixed into 15 mL ethanol with vigorous stirring to get a homogeneous suspension. Resulting suspension in brown colour was transferred into a 45 mL Teflon-lined stainless steel autoclave and heated at 180 ^{o}C for 18 h. After naturally cooling down to room temperature, the precipitate was collected by vacuum filtration, rinsed three times with deionized water, and finally dried under vacuum at 80 ^{o}C for overnight. Crystal structure of the product was identified by X-ray diffraction (XRD) using an X-ray diffractometer (Rigaku Ultima III) with Cu-Kα radiation (λ = 1.5418 Å) from 20° to 55° at a scanning rate of 1° min^{-1}. Morphology was observed and photographed using a Quanta 200F scanning electron microscope.

2.2. Electrochemical measurements

The resultant CP@FeS powder was coated onto a carbon-coated aluminium foil at a weight ratio of 75% CP@FeS, 10% Super-P carbon, 10% Ketjenblack EC-300JD carbon black and 5% binder by using poly(acrylonitrile-methyl methacrylate) (ANMMA, AN/MMA= 94:6, MW=100,000, Polysciences, Inc.) as the binder and N-methyl pyrrolidinone as the solvent. On average, the electrode had a loading of 2 mg CP@FeS per cm^2. The electrode was punched into 1.27 cm^2 circular discs and dried at 80 °C under vacuum for 16 h. Two solutions, one consisting of 1.0 m lithium bis(trifluoromethanesulfonyl)imide (LiTFSI) dissolved in a 1:1 (wt.) mixture of dimethyl ether (DME) and 1,3-dioxolane (DOL) and the other consisting of 1.0 m $LiPF_6$ dissolved in a 3:7 (wt.) mixture of ethylene carbon (EC) and ethylmethyl carbonate (EMC), were used as the electrolyte. Using a Celgard 3410 membrane as the separator, 2032-size coin cell was assembled and filled with 20 μL electrolyte. Cyclic voltammetry was measured at 0.1 mV s^{-1} on a Solartron SI 1287 Electrochemical Interface, and the cell was cycled between 1.0 V and 2.3 V (or 2.6 V) on a Maccor Series 4000 cycler. The specific capacity was expressed with respect to the mass of CP@FeS microcrystals.

3. Results and discussion

3.1. Structure and chemical stability of FeS

In this work, we originally attempted to coat a conductive carbon layer onto the surface of FeS particles by using the solvothermal pyrolysis of sucrose. Unfortunately, Raman spectrum of the product only shows a broad D-band absorbance in the 1250-1500 cm^{-1} region (Fig. S1), indicating that the solvothermal process only led to the formation of a carbon precursor. Therefore, we refer to our product as the carbon-precursor coated iron monosulphide (CP@FeS). Fig. 1a and Fig. 1b show the XRD patterns of CP@FeS powder before and after being stored in a sealed vial for 5 weeks. As shown in Fig. 1a, the as-prepared CP@FeS consists of two FeS phases, one indexed to JCPDF #01-089-6926 and the other indexed to JCPDF #01-089-6272, and contains small amount of elemental sulphur. The co-existence of two FeS phases agrees with the fact that FeS precipitated from the aqueous Fe^{2+} and S^{2-} solutions is a polycrystalline and nonstoichiometric compound, namely Fe_mS with m=0.91~1.15 or FeS_n with n=0.87~1.10.[7] It has been reported that annealing the product at 400~600 ^{o}C in an inert atmosphere may lead to a single phase,[13-15] however, sulphur impurity is still detectable by the XRD.[14] In our case, we consider that sulphur is formed probably through two routes during the post-treatment in air: One is the oxidization of excess Na_2S since in our synthesis twice calculated moles of Na_2S were used for the purpose to protect the reductive Fe^{2+} from being oxidized and the other is the oxidization of the resultant FeS in air according to the reaction below.[7, 15]

$$FeS + 1/2O_2 \rightarrow FeO + 1/8S_8 \quad [1]$$

In fact, pure FeS phase has never been reported to be precipitated from the aqueous solutions.[7] X-ray photoelectron spectroscopy (XPS) indicates that the surface of FeS particles inevitably contains some of Fe^{3+} and O^{2-} ions (namely the formation of FeO and Fe_3O_4).[12, 13, 15] After 5 weeks storage in a sealed vial, the sample was re-checked again using XRD. To our surprise, the FeS phases were entirely converted to Fe_3S_4 phase (JCPDF #01-089-1999) accompanied by the vanishing of sulphur characteristic peaks, as shown in Fig. 1b. The Fe_3S_4 is additionally identified by the strong magnetic property as depicted in Fig. S2. The above facts reveal the following transformation has occurred during the storage.

$$3FeS + 1/8S_8 \rightarrow Fe_3S_4 \quad [2]$$

It should be noted that Fe_3S_4 is thermodynamically metastable, which transforms to more stable FeS_2 under hypoxic condition or is oxidized to form sulphur under aerobic condition.[7, 16] However, this is beyond the scope of the present work. Fig. 1c shows SEM image of the CP@FeS sample after 5 weeks storage. It is indicated that most of Fe_3S_4 particles are smaller than 1 μm in diameter and the particle size is distributed broadly. The wide particle size distribution is because the precipitation of FeS particles was dominated by the nucleation process in the process of mixing the Fe^{2+} and S^{2-} solutions. The Fe_3S_4 particles also show some degree aggregation with many small secondary particles embedded on the surface of the primary particle.

Cite this: DOI: 10.1039/c0xx00000x

www.rsc.org/xxxxxx

PAPER

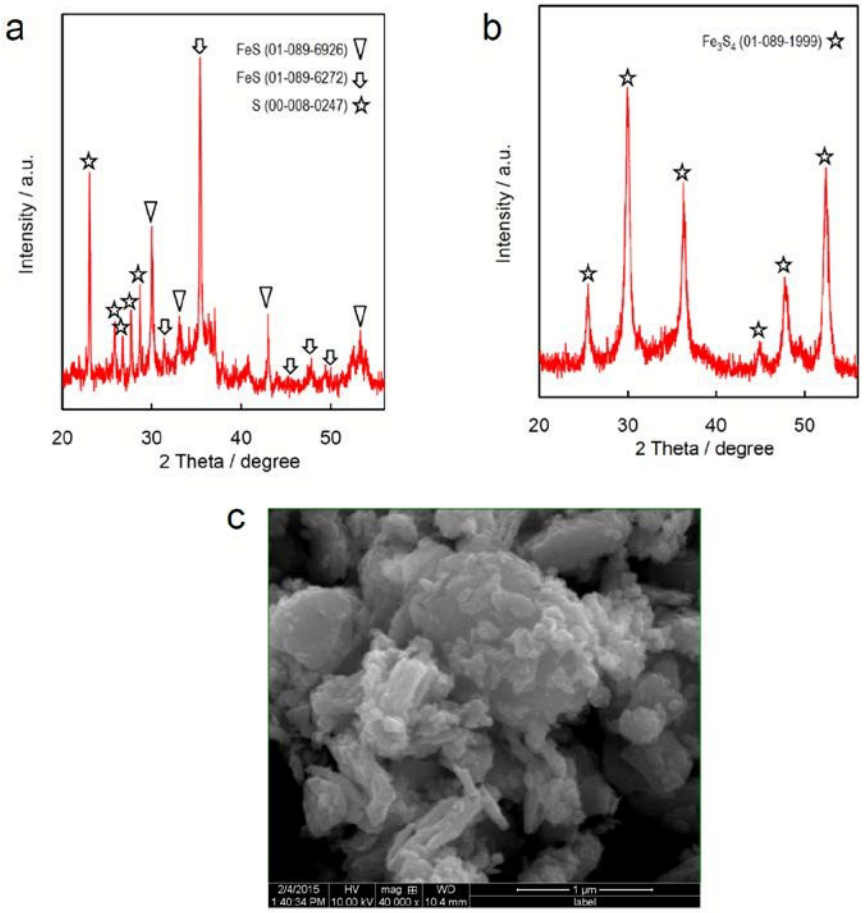

Fig. 1 (a) XRD pattern of as-prepared CP@FeS, (b) XRD pattern of CP@FeS after being stored in a sealed vial for 5 weeks, and (c) SEM image of CP@FeS after being stored in a sealed vial for 5 weeks.

3.2. Redox mechanism of FeS

Typical cyclic voltammograms of the first two cycles of a Li/FeS cell are displayed in Fig. 2. In the first discharge scanning from the open-circuit voltage (~3 V), there are at least three reduction current peaks above 1.4 V. The current peak marked by the red solid triangle is assigned to the reduction of Fe^{3+} to Fe^{2+} in Fe_3S_4, and the other two peaks to the reduction of short-chain polysulphide formed during the synthesis and storage. The major current peak at 1.3 V is assigned to the reversible reduction of FeS, namely eq. 3.

$$FeS + 2Li \leftrightarrow Fe + Li_2S \quad [3]$$

$$nLi_2S \leftrightarrow (2n-2)Li + Li_2S_n \quad [4]$$

The subsequent charge scanning shows a major oxidization current peak at ~2 V. Since the potentials for the oxidization of Fe (i.e., the reverse of eq. 3) and Li_2S (eq. 4) are very close, eq. 4 and the reverse of eq. 3 often take place in parallel. Therefore, the recharging leads to a mixed product of the FeS and Li_2S_n and in the extreme case elemental sulphur can be formed by eq. 4. The very small current peak at ~2.4 V is ascribed to the oxidization of soluble Li_2S_8 to insoluble S_8,[17] which vanishes quickly with cycle number as a result of the progressive loss of sulphur species from the cathode.

Cyclic voltammogram of the 2nd cycle becomes normal, but does not reproduce that of the 1st discharge. In particular, the current peak for the reduction of Fe^{3+} to Fe^{2+} permanently vanishes. There are only two reduction current peaks, the small one starting at about 2 V for the reverse of eq. 4 and the large one starting at 1.5 V for eq. 3, which are in excellent agreement with those reported elsewhere.[3, 11-15] This fact clearly reveals that the transformation of FeS to Fe_3S_4 as well as the oxidization of FeS and Fe_3S_4 to sulphur accompanied by the formation of FeO and Fe_3O_4 only affects the first discharge voltage profile with negligible impact on the subsequent cycling.

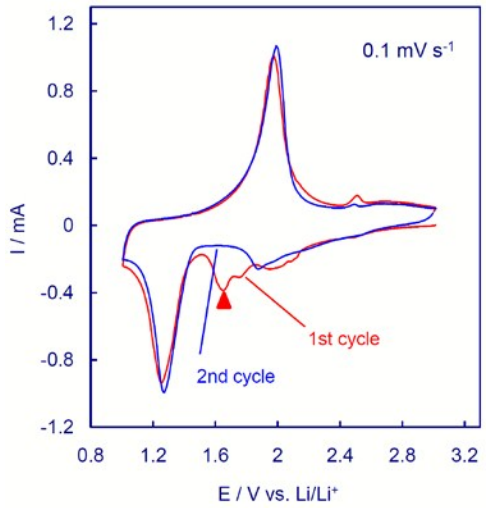

Fig. 2 Cyclic voltammograms of the first two cycles of a Li/FeS cell using a 1.0 m LiTFSI 1:1 DME/DOL electrolyte.

Fig. 3 shows the voltage profile and voltage dependence of differential capacity for the first two cycles of a Li/FeS cell using the newly coated FeS cathode. The voltage profile and voltage dependence of differential capacity well coincide with the cyclic voltammogram results (Fig. 2). As indicated by the five-star and triangle marks in Fig. 3b, the first discharge exhibits some capacities of the short-chain polysulphide and Fe^{3+} ions, respectively, before the major capacity of FeS is accessed at ~1.4 V. There is a significant loss in the capacity from the 1st discharge to the 2nd discharge (see Fig. 3a). This is a common phenomenon for all types of transition metal sulphides,[3, 18] and is believed to be associated with the low charging efficiency of Li_2S (eq. 4) and the loss of sulphur species as a result of the dissolution of long-chain lithium polysulphide. As indicated by Fig. 3b, in the 2nd discharge there are no characteristic differential capacity peaks around 2.4 V and 2.0 V of elemental sulphur, indicating that the Li_2S is only charged to such a state that the Li_2S_n in eq. 4 are in short chains. Therefore, the initial capacity loss from the 1st discharge to the subsequent recharge can be attributed to the insufficient oxidation of Li_2S and the loss of sulphur species. As shown by Fig. 3a, the 2nd discharge does not reproduce the voltage profile of the 1st discharge whereas that of the 2nd discharge is repeatedly reproduced by the subsequent discharges (not show in Fig. 3a). The above results reveal that the recharge does not reconstitute the original structure once the FeS (and Fe_3S_4) is fully discharged, being very similar to those observed from the Li/FeS_2 batteries.[18] In the 2nd discharge of Fig. 3a, the upper sloping voltage regions (namely those above 1.5 V plateau) are assigned to the reduction of short-chain Li_2S_n, and the 1.5 V voltage plateau to the reduction of FeS.

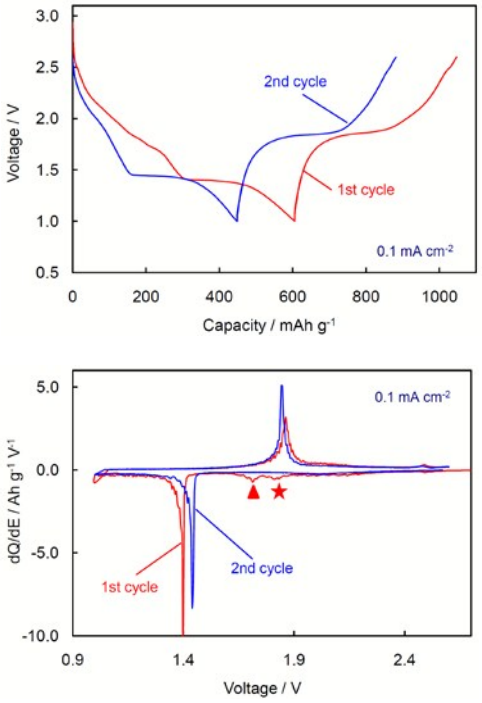

Fig. 3 Cycling performance of the first two cycles for a Li/FeS cell using a newly coated cathode. (a) Voltage profile, and (b) differential capacity-voltage plot.

3.3 Factors to affect performance of FeS cathode

3.3.1. Exposure to air

Fig. 4 shows the cycling performance of the first two cycles for a Li/FeS cell using the cathode having been exposed to air for 5 weeks in a dry room. Compared with Fig. 3b, the first discharge in Fig. 4b shows two additional capacity peaks at 2.4 V and 2.2 V, respectively, as indicated by two hollow arrows. The potentials of these two discharge capacity peaks well coincide with those of elemental sulphur.[17] This observation can be attributed to the fact that the metastable Fe_3S_4 is irreversibly oxidized by oxygen in air to form sulphur, as described by eq. 5:[7, 16]

$$Fe_3S_4 + 2O_2 \rightarrow Fe_3O_4 + 1/2S_8 \quad [5]$$

Since both of the resultant Fe_3O_4[19, 20] and sulphur[17] in eq. 5 are electrochemically active and their reductions yield the same products as Fe_3S_4 does (i.e., forming Fe and Li_2S), the oxidization of Fe_3S_4 is considered not to affect the specific capacity and cycling performance of the subsequent cycling.

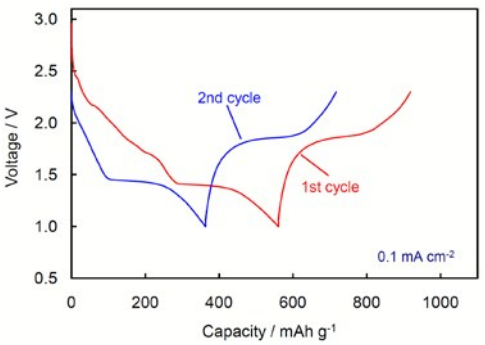

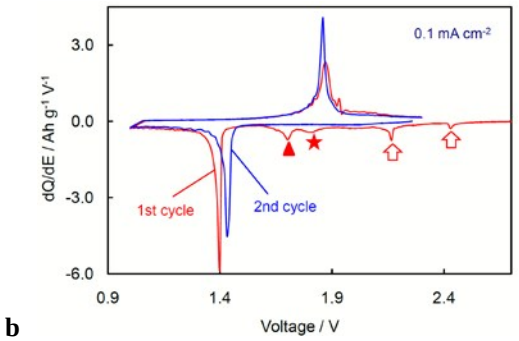

Fig. 4 Cycling performance of the first two cycles for a Li/FeS cell using a cathode having been exposed to air for 5 weeks in a dry room. (a) Voltage profile, and (b) differential capacity-voltage plot.

3.3.2. Electrolyte solvent

As discussed above, the oxidization of Li_2S (i.e., eq. 4) is inevitably involved in the charging process of the Li/FeS cells. Therefore, the same problems as observed from the Li/S batteries are also present in the Li/FeS battery. Fig. 5 exhibits the effect of electrolyte solvents on the cyclability for a Li/FeS cell with the CP@FeS cathode having been exposed to air for 5 weeks. When a EC/EMC electrolyte is used, the voltage profile (Fig. 5a) and differential capacity-voltage plot (Fig. 5b) of the first two cycles become much more complicated as compared with those of the DME/DOL electrolyte (Fig. 4a and Fig. 4b). In particular, the differential capacity-voltage plots show many irregular capacity peaks (see Fig. 5b), suggesting that parasitic reactions take place in the discharging and charging processes. According to previous reports on the Li/S batteries,[21, 22] these reactions are attributed to the nucleophilic reaction between the polysulphide anions and carbonate solvents. As a result, Fig. 5c shows that the cell with the EC/EMC electrolyte suffers from much faster capacity fading and always has an about 2% lower coulombic efficiency as compared with the counterpart using the DME/DOL electrolyte. The above results reveal that the Li/FeS batteries are preferential to the ether-based electrolytes. In addition, Fig. 5d compares the voltage profiles of 100th and 200th cycles for a Li/FeS cell using a 1.0 m LiTFSI 1:1 DME/DOL electrolyte. It is shown that the loss of discharge capacity from 100th to 200th cycle mainly occurs in the 1.5 V plateau, namely the process corresponding to eq. 3. This can be attributed to the progressive growth in the particle size of metallic Fe and Li_2S, which consequently results in a decrease in the utilization of active cathode material.

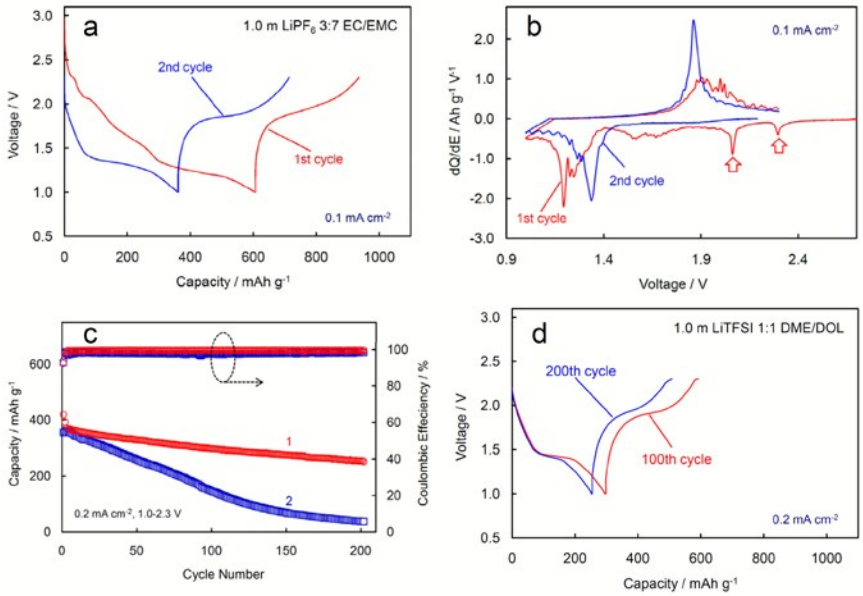

Fig. 5 Cycling performance of a Li/FeS cell using a 1.0 m $LiPF_6$ 3:7 EC/EMC electrolyte. (a) Voltage profile of the first two cycles, (b) differential capacity-voltage plot of the first two cycles, (c) cycling performance of two Li/FeS cells using (1) 1.0 m LiTFSI 1:1 DME/DOL and (2) 1.0 m $LiPF_6$ 3:7 EC/EMC, respectively, and (d) voltage profile of the 100th and 200th cycle for a Li/FeS cell using a 1.0 m LiTFSI 1:1 DME/DOL electrolyte.

3.3.3. Charging cutoff voltage

As discussed in Section 3.2, the Li/FeS battery shares many commonalities in the redox mechanism with the Li/FeS_2 batteries that have been discussed in a recent review article.[18] In the same manner used for the Li/FeS_2 batteries, the charging cutoff voltage can be controlled to reduce the formation of soluble (long-chain) lithium polysulphide. Fig. 6 displays the effect of charging cutoff voltage on the capacity retention of the Li/FeS cells using two different types of electrolytes. In both cases, raising the cutoff voltage increases the capacity while accelerating the fading of capacity because at high voltage the Li_2S can be charged to longer chain Li_2S_n or even elemental sulphur, which enhances both the utilization of sulphur active material and the dissolution of Li_2S_n in the electrolyte. In contrast, the low cutoff voltage (2.3 V) leads to better capacity retention with modest lower capacity because the low cutoff voltage reduces the formation of long-chain Li_2S_n, and consequently the loss of sulphur species in relation to the dissolution of long-chain Li_2S_n. We believe that the present strategy is also applicable to other transition metal sulphides.

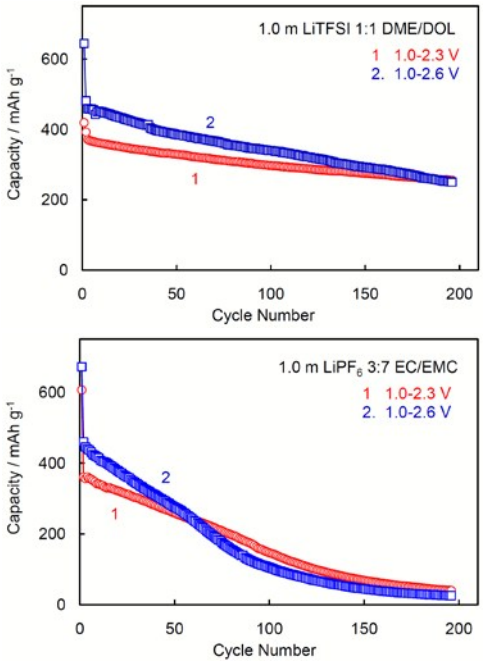

Fig. 6 Effect of charging cutoff voltage on the capacity retention of Li/FeS cells. (a) 1.0 m LiTFSI 1:1 DME/DOL electrolyte, and (b) 1.0 m $LiPF_6$ 3:7 EC/EMC electrolyte.

3.3.4. Rate capability

Fig. 7 depicts the rate capability of a Li/FeS cell employing a 1.0 m LiTFSI 1:1 DME/DOL electrolyte, which was recorded by charging the cell at 0.2 mA cm^{-2} and discharging at different current densities. Although the cell is charged and discharged at different current densities, it is shown that all cycles have a near 100% coulombic efficiency. The specific capacity of CP@FeS at 0.1 mA cm^{-2} reaches 550 mAh g^{-1} (equal to 90% of the theoretical value) in the 1st discharge, and declines to 370 mAh g^{-1} in the 2nd discharge. The capacity still retains at 285 mAh g^{-1} (77% of the 2nd discharge capacity at 0.1 mA cm^{-2}) with small polarization in the discharge voltage even when the current density rises to 3.0 mA cm^{-2}. The excellent rate capability is attributed to one hand the small CP@FeS particle size (<1 μm) that shortens the diffusion distance of Li^+ ions in the cathode reaction and the other hand the formation of metallic Fe that is embedded in the insulating Li_2S matrix to form the highly conductive networks.

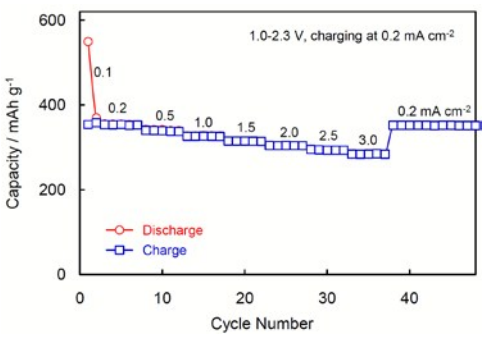

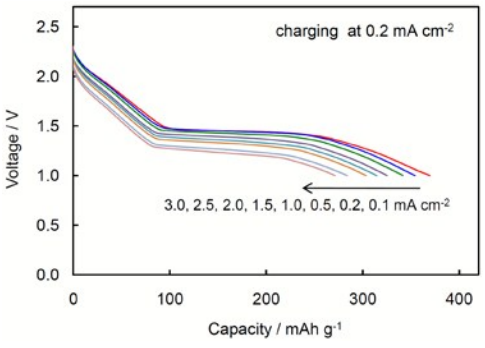

Fig. 7 Rate capability of the Li/FeS cell with a 1.0 m LiTFSI 1:1 DME/DOL electrolyte. (a) discharge and charge capacities, and (b) discharge voltage profile at different current densities.

4. Conclusions

In summary, the FeS precipitated by mixing the aqueous Fe^{2+} and S^{2-} solutions is a mixture of two FeS phases and contains small amount of sulphur. In storage, the mixture transforms to metastable Fe_3S_4 that can be further oxidized by oxygen in air to form sulphur accompanied by the formation of Fe_3O_4. However, such transformation and oxidization only affect the first discharge voltage profile with negligible impact on the specific capacity and performance of the subsequent cycling. Except for the first discharge, subsequent cycling of the Li/FeS cells is performed through two redox couples of the Li_2S/Li_2S_n for the higher voltage region and the Fe/FeS for the lower 1.5 V voltage plateau. The Li/FeS batteries favour ether-based electrolytes. Lowering the charging cutoff voltage reduces the formation of soluble (long-chain) Li_2S_n, and hence increases the capacity retention of the Li/FeS batteries. This strategy can be extended to other transition metal sulphides.

Notes and references

[a] *Energy and Power Division, Sensors and Electron Devices Directorate, U.S. Army Research Laboratory, Adelphi, MD 20783-1138, USA. Fax: 1-301-394-0273; Tel: 1-301-394-0981; Email (S. S. Zhang): shengshui.zhang.civ@mail.mil, or shengshui@gmail.com*

1. S. S. Zhang, *Front. Energy Res.*, 2013, **1**. 8. doi: 10.3389/fenrg.2013.00008.
2. W. L. Bowden, L. H. Barnette and D. L. Demuth, *J. Electrochem. Soc.*, 1988, **135**, 1− 6.
3. Y. Kim and J. B. Goodenough, *J. Phys. Chem. C*, 2008, **112**, 15060−15064.
4. C. H. Lai, M. Y. Lu and L. J. Chen, *J. Mater. Chem.*, 2012, **22**, 19−30.
5. X. Zhou, L. J. Wan and Y. G. Guo, *Chem. Commun.*, 2013, **49**, 1838−1840.
6. Y. Du, X. Zhu, X. Zhou, L. Hu, Z. Dai and J. Bao, *J. Mater. Chem. A*, 2015, **3**, 6787−6791.
7. D. Rickard and G. W. Luther, *Chem. Rev.*, 2007, **107**, 514−562.
8. C. H. W. Jones, P. E. Kovacs, R. D. Sharma and R. S. Mcmillan, *J. Phys. Chem.*, 1990, **94**, 4325−4329.
9. S. H. Kim, Y. J. Choi, D. H. Kim, S. H. Jung, K. W. Kim, H. J. Ahn, J. H. Ahn and H. B. Gu, *Surf. Rev. Lett.*, 2008, **15**, 35−40.
10. M. Akhtar, J. Akhter, M. A. Malik, P. O'Brien, F. Tuna, J. Raftery and M. Helliwell, *J. Mater. Chem.*, 2011, **21**, 9737−9745.
11. B. Wu, H. Song, J. Zhou and X. Chen, *Chem. Commun.*, 2011, **47**, 8653−8655.

12. C. Xu, Y. Zeng, X. H. Rui, N. Xiao, J. X. Zhu, W. Y. Zhang, J. Chen, W. L. Liu, H. T. Tan, H. H. Hng and Q. Y. Yan, *ACS Nano.*, 2012, **6**, 4713−4721.
13. X. Wang, Q. Xiang, B. Liu, L. Wang, T. Luo, D. Chen and G. Shen, *Sci. Rep.*, 2013, **3**. doi: 10.1038/srep02007.
14. L. Fei, Q. Lin, B. Yuan, G. Chen, P. Xie, Y. Li, Y. Xu, S. Deng, S. Smirnov and H. Luo, *ACS Appl. Mater. Inter.*, 2013, **5**, 5330−5335.
15. C. Dong, X. Zheng, B. Huang and M. Lu, *Appl. Surf. Sci.*, 2013, **265**, 114−119.
16. A. P. Roberts, L. Chang, C. J. Rowan, C. S. Horng and F. Florindo, *Rev. Geophys.*, 2011, **49**, RG1002.
17. S. S. Zhang, *J. Power Sources*, 2013, **231**, 153−162.
18. S. S. Zhang, *J. Mater. Chem. A*, 2015, **3**, 7689−7694.
19. G. Zhou, D. W. Wang, F. Li, L. Zhang, N. Li, Z. S. Wu, L. Wen, G. Q. Lu and H. M. Cheng, *Chem. Mater.*, 2010, **22**, 5306−5313.
20. B. Li, H. Cao, J. Shao and M. Qu, *Chem. Commun.*, 2011, **47**, 10374−10376.
21. J. Gao, M. A. Lowe, Y. Kiya and H. D. Abruña, *J. Phys. Chem. C*, 2011, **115**, 25132−25137.
22. T. Yim, M. S. Park, J. S. Yu, K. J. Kim, K. Y. Im, J. H. Kim, G. Jeong, Y. N. Jo, S. G. Woo, K. S. Kang, I. Lee and Y. J. Kim, *Electrochim. Acta*, 2013, **107**, 454−460.